Deformable Mirror Development at Stanford University

Justin D. Mansell[*a], Supriyo Sinha[**b], and Robert L. Byer[b]
[a]Intellite, Inc.; [b]Ginzton Laboratory, Stanford University

ABSTRACT

High power lasers often suffer from phase aberrations due to spatially non-uniform temperature distributions in optical elements. Adaptive optics has been established to provide engineering control over phase aberrations, but it has been mostly applied to astronomy and has been too costly to use in commercial lasers. The goal of our research has been to develop low-cost adaptive optics systems and components for laser aberration compensation. We present here a summary of our adaptive optics work and our vision of the future of adaptive optics.

Keywords: deformable mirrors, lasers, adaptive optics

INTRODUCTION

Our initial motivation for this research on adaptive optics was to control the laser wavefront for the Laser Interferometer Gravitational-Wave Observatory (LIGO). LIGO is a large optical interferometer designed to measure gravitational wave radiation.[1] Figure 1 shows a simplified optical schematic of LIGO. The LIGO optical setup is basically a Michelson interferometer with linear Fabry-Perot cavities in each of the arms. An Nd:YAG laser light is amplified and then transmitted through a set of conditioning optics including lenses, a Faraday isolator, and an electro-optic modulator before illuminating the Fabry-Perot ring mode cleaners. Each Fabry-Perot mode cleaner temporally and spatially filters the laser beam to reduce the amplitude noise and to eliminate the higher-order spatial mode content on the beam. The resonant cavities are called mode cleaners because they filter out most of the higher-order spatial modes of the beam before illuminating the LIGO Michelson interferometer.

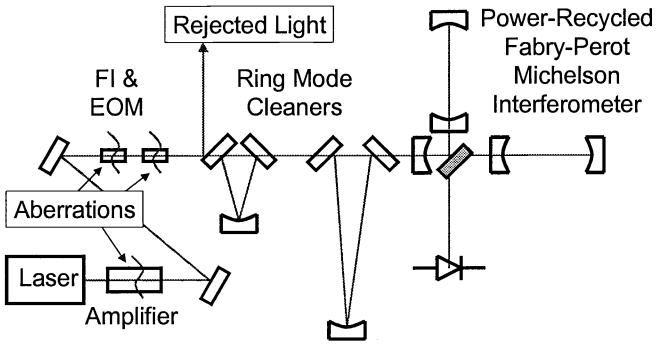

Figure 1 - **Simplified optical layout of the LIGO interferometer.**

During operation, the arms of the interferometer are locked in length so that the port with the photodiode undergoes destructive interference and therefore is dark. A power-recycling mirror reflects the light from the bright port back into the interferometer to increase the circulating optical power, and therefore increase the sensitivity of the interferometer. An incoming gravitational wave induces an effective change in the optical path length of one arm relative to the other, thus causing an intensity fluctuation on the photodiode. The weak interaction of gravitational wave radiation with light induces a change of less than one part per billion in the optical phase or 10^{-10} radians.

The sensitivity of the interferometer to gravitational wave radiation is proportional to the amount of light on the beam splitter. Since the interferometer is comprised of a set of optical cavities, ideally only a perfect gaussian beam is accepted into the interferometer. Aberrations induced in the conditioning optics and in the laser amplifier before the interferometer cause light to be rejected from the interferometer and thus reduce the sensitivity of the interferometer. The thermally-induced aberrations in the optics before the interferometer are static assuming the laser power is constant, but ramping up the laser power and the slow decrease of the laser power due to deterioration of the laser diodes cause the aberrations to change with time. Since there is no way of predicting the occurrence of a gravitational wave, the

* jmansell@intellite.com; phone 1 505 268-4742; fax 1 505 268-4741; http://www.intellite.com; Intellite, Inc., 1717 Louisiana Ste. 202, Albuquerque, NM, USA 87110; ** supriyo@stanford.edu; phone 1 650 725-2266; fax 1 650 725-2666; http://www.stanford.edu/~supriyo; Stanford University, 450 Via Palou, Stanford, CA, USA 95305.

High-Resolution Wavefront Control: Methods, Devices, and Applications III, John D. Gonglewski, Mikhail A. Vorontsov, Mark T. Gruneisen, Editors, Proceedings of SPIE Vol. 4493 (2002)

interferometer must be on all the time for several years to increase the chance of an observation. Thus, the aberrations must be actively compensated to maintain continuous operation of the observatory.

The LIGO Nd:YAG laser begins with a non-planar ring oscillator (NPRO)[2] that generates a beam with the majority of its power in the lowest-order Hermite-Gaussian spatial mode. Aberrations induced by the laser amplifier and the transmissive optics, like the Faraday isolator, the electro-optic modulators, and even the lenses cause light to be reflected from the mode cleaners and not reach the interferometer. These aberrations are mostly caused by a non-uniform temperature distribution in the optics. In laser amplifiers this non-uniform temperature distribution is caused by non-uniform optical absorption and the inability to extract the heat uniformly.

The optical path length through any optic is a product of the refractive index and the distance the light travels through the material. The temperature change affects both of these parameters. The distance the light travels through the material can change due to thermal expansion of the material, but in transmissive optics the larger effect is usually the change in refractive index with respect to temperature. The spatially distributed change in the optical path length is often referred to as "thermal lensing" because it is mostly parabolic, like an ideal lens. Unfortunately, these thermal lenses are rarely exclusively parabolic, therefore they cause coupling of the laser light into higher-order spatial modes and therefore deterioration in the laser beam quality. These aberrations cause laser power to be reflected from the interferometer and thus reduce its sensitivity. Our goal is to use adaptive optics to keep as much laser power as possible in the interferometer to maximize its sensitivity.

We examined the possibility of using existing components for the LIGO adaptive optics system and discovered that many of the existing technologies were either not well adapted to laser adaptive optics or prohibitively expensive. We began by adapting Shack-Hartmann wavefront sensor technology to lasers by developing a technique for apodizing the micro-lens arrays.[3] After evaluating different deformable mirror technologies, we decided to develop a low-cost deformable mirror designed for high laser power using micromachining. Several other applications were kept in mind during this development so that the resulting deformable mirror architecture would have applicability outside the high-power laser community.

In this paper we will describe ideal deformable mirror characteristics and how each of the commercially available technologies did not meet our criteria. Then we will describe the two-layer and three-layer two different deformable mirror architectures and one additional deformable mirror developed for a spectroscopy application. We will conclude by discussing some of our current work.

IDEAL DEFORMABLE MIRROR CHARACTERISTICS

Ideal characteristics for deformable mirrors were established in the literature during the development of adaptive optics systems for astronomy in the 1970s.[4] Some of the characteristics stemmed from a basic understanding of optics. The mirror surface should have high reflectivity and low optical loss, thus necessitating a polished and coated mirror surface. Aberrations that developed during fabrication of the mirror should be compensated with the mirror actuators. The response to voltage will ideally be linear, but simple non-linearities are acceptable.

More detailed mirror characteristics were derived from an understanding of the atmosphere presented by Kolmogorov.[5] Based on Kolmogorov's model of the atmosphere, the adaptive optics community developed a characteristic size given by Fried's coherence length (r_0),[6] typically around 10cm, and a characteristic time constant given by the reciprocal of the Greenwood frequency,[7] which is typically around 50Hz. Control theory says that the the first mechanical resonance of the mirror should be about one order of magnitude above the Greenwood frequency for sufficient control of the system. Furthermore, there should be roughly one actuator corresponding to each patch of sky equal in size to Fried's coherence length. Continuing the use of the Kolomogorov atmospheric turbulence model, Hudgin studied the optimal actuator influence function, which is the shape of the distortion an individual mirror actuator creates on the mirror surface.[8] Hudgin reported that to achieve equivalent residual wavefront error, almost 8 times more actuators were required if their influence functions were piston-only instead of gaussian in shape. Further work in the literature has shown a variety of different results in this regard, but there is always a significant improvement in modeled systems when a continuous influence function is used.[4] Finally, Tyson studied the ideal amount of crosstalk between adjacent actuators for compensating atmospheric aberrations and found an optimum around 15%.[9]

Adaptive optics systems designed for lasers impose a new set of requirements on the deformable mirror. The mirror surface has to be specially designed to handle laser power, which means low roughness, high flatness, and the ability to be coated with a multi-layer dielectric. Although flatness and roughness are similar, the distinction in optics is the spatial scale. For discussing deformable mirrors, we designate aberrations with spatial period less than double the mirror actuator spacing as roughness and those with larger spatial period as flatness. Deformable mirrors can actively flatten themselves in the right control loop, but they cannot compensate for roughness problems. Low roughness is required to avoid scattering light from the primary beam. With enough throw, flatness can be obtained in any deformable mirror, but it reduces the usable mirror throw. Beyond the strict surface shape requirements, the surface must be able to handle laser power without damaging or distorting beyond the mirrors ability to compensate its own thermally induced distortions and the distortions it is being implemented to correct. The mirror should be capable of being coated with a high-reflectivity low-absorption coating to handle the laser power. For low-power laser applications, metal coatings are acceptable, but a multi-layer dielectric coating will be required for high laser power because absorption will either excessively distort the mirror surface or cause damage.

DESCRIPTION AND EVALUATION OF EXISTING SPATIAL PHASE MODULATORS

Table 1 summarizes a comparison of some of the known spatial phase modulator technologies with the ideal specifications of a spatial phase modulator. A discussion of the drawbacks of each technology, italicized in Table 1, is presented in the following paragraphs.

Conventional Deformable Mirrors

Deformable mirrors formed with piezoelectric or electrostrictive actuators on a glass plate are the oldest and the most commonly used in adaptive optics systems today. The major disadvantage is the lack of scalablity. These devices are fabricated by attaching an array of actuators to the back of a thin mirror by hand. This fabrication technique leads to large variability in device performance and no potential for achieving very large numbers of actuators at any reasonable cost. Furthermore, the actuator response is very temperature sensitive.

Liquid Crystals

Liquid crystals offer a great deal of advantages to adaptive optics, but they offer no obvious way to address high bandwidth applications and offer very limited throw. Furthermore, the liquid crystal spatial phase modulators have never been very good at handling laser power due to their absorbing indium tin oxide (ITO) transparent electrode. Recent data from Livermore National Laboratories shows that the damage threshold of their liquid crystal spatial phase modulators is about $16W/cm^2$ for 1064nm light. Temperature dependence of the liquid crystal material makes it necessary to have some limited thermal range. Finally, chromatic and polarization effects limit their performance for some applications.

Micromachined Deformable Mirrors

Silicon micromachining can be divided into surface micromachining techniques and bulk micromachining techniques. Surface micromachining involves adding layers of different materials to a wafer surface and then using a wet etchant to remove one type of layer and release the structure. In the typical case where these layers are polysilicon and silicon dioxide, the wet etchant is hydrofluoric acid.

Table 1 - Spatial Phase Modulator Characteristics

Characteristic	Ideal DM	PZT or PMN	Surface MEMS	Membrane DMs	Liquid Crystal
Throw (μm)	Large	4	~1	~10	~1
Spacing(mm)	Small	*7*	0.3	2	~0.1
Crosstalk	Low	Low	Low	*High*	Low
Influence Function	Smooth	Smooth	Smooth	Smooth	*Piston*
Cost	Low	*$1000 / actuator*	Low	Low	Low
Pixel Flatness	λ/50	Good	*Poor*	Good	Good
Roughness	Low	Low	*High*	Low	Low
Scalable to 1M Actuators	Yes	*No*	Yes	*No*	Yes
Circuitry Integration	Yes	*No*	*Maybe*	Yes	*Maybe*
Laser Power Handling	High	Good	*Poor*	Medium	*Poor*
Response Time (μs)	10	1000	15	1000	*10,000*
Fabrication Complexity	Low	*High*	Low	Low	Low
Thermal Variations	Zero	*High*	Low	Low	*Medium*
Response to Voltage	Linear	Linear	Parabolic	Parabolic	*Nonlinear*

Surface Micromachining

Many researchers have investigated surface micromachined deformable mirrors because they can be fabricated at foundries instead of requiring months of work in a clean room to get devices.[10,11] Although surface micromachining offers a very quick way to test architectures, sometimes the limitations of the process are critical to the success of a device. The surface quality of these devices has been poor due to the segmentation and perforation of the mirror surface. This perforation cannot be circumvented in the conventional surface micromachined process because a wet release must be able to enter the structure through the mirror surface. These perforations create high absorption points in the mirror and seed laser-induced damage.

Another limitation of surface micromachining is the inability so far to easily integrate complex silicon circuitry with surface micromachined devices. This leads to large numbers of densely packed wires on a wafer, which could provide a fundamental limit to the scaling of these mirrors to large sizes. In addition to the large numbers of wires on a surface micromachined wafer without any circuitry, there is the further problem of getting connections to these wires off the chip. Finally, accumulated roughness and stresses induced during deposition of the layers make it difficult to achieve high quality mirror surfaces, even if the wafer is polished before the wet etch release step.[11]

Typical foundry surface micromachining, like that used by Boston University and Boston Micromachines, has a limited thickness and therefore a limited throw. A recent advance in surface micromachining from Lucent has demonstrated the ability to achieve longer throw surface micromachined devices by exploiting the difference in stresses of two coatings. Upon release, the Lucent mirrors lift above the surface allowing for a wider range of tilt. The disadvantage of this technology is that the differential stress elements used for lifting the mirror are temperature sensitive.

Bulk Micromachining

Bulk micromachining always involves deep etches into the wafer, often completely through the wafer. When done properly, the deep etch enters the back of the mirror and leaves the front reflective surface untouched during processing.

Typically long etches in tetra-methyl ammonium hydroxide (TMAH) or potassium hydroxide (KOH) are used for removing large amounts of silicon with silicon nitride or silicon dioxide as an etch mask. Bulk micromachining offers the ability to achieve a continuous membrane surface, which would alleviate scattering problems with surface micromachining. Unfortunately the majority of the mirrors to date made using this technology do not have any way of being scaled to large aperture because the mirror resonance frequency scales with the mirror area. Furthermore, the cross talk between actuators is high, thus preventing higher order correction. Similar problems are the fundamental limitations of bimorph mirror architectures. Finally, current bulk micromachined deformable mirrors are typically destroyed during electrostatic snap-down, which occurs when the electrostatic force exceeds the mechanical restoring force and the mirror collapses into the underlying pad arrays.

Many people cite the need for a clean room and the fabrication complexity of bulk micromachining as a drawback, but we have found the limitations of surface micromachining foundries to be a bigger problem. We have found that many complex structures can be made in even a simple clean room with 1970's class equipment. Complex steps like epitaxial silicon growth or silicon nitride deposition can be sent out to a number of different foundries for minimal cost. Simple steps like lithography can be performed in a number of small clean rooms nationwide. Finally, the cost of setting up a small clean room for bulk micromachining is typically under $750,000 and several of these clean rooms allow users to lease space for very reasonable rates.

THE SILICON NITRIDE TWO-LAYER DEFORMABLE MIRROR ARCHITECTURE

We began our investigation with a two-layer deformable mirror architecture as a stepping-stone to the three-layer architecture. We have chosen the nomenclature two-layer instead of membrane because some of our two-layer mirror architectures use thick plates as the upper surface.

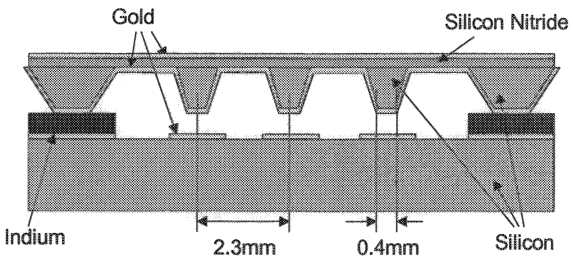

Figure 2 - Cross sectional view of deformable mirror architecture.

Figure 2 shows a cross-section of the second two-layer mirror architecture we built. We changed the fabrication of the two-layer architecture from prior work by replacing the silicon mirror with a silicon nitride mirror to achieve better mirror flatness.[12] The deformable mirror is comprised of a silicon wafer piece bonded to an array of electrodes on a separate silicon wafer piece. The mirror is comprised of a thin tensile mirror membrane coated with a metallic reflector and held by a silicon frame. Silicon pillars coated with a thin layer of gold attached to the back surface extend down toward a corresponding array of electrostatic pads on the second piece. The mirror operates by applying a bias to the mirror and applying voltage to each of the corresponding pads to cause a potential difference between the pillar tips and the pads and induce electrostatic attraction. This provides a mechanism for controlling the shape of the mirror surface and thus the wavefront of a beam of light reflected from the mirror. Figure 3 shows a photograph of the two-layer deformable mirror after fabrication.

Figure 3 - Photograph of the two-layer silicon deformable mirror with a standard 2 mm ribbon cable connector next to a US quarter.

Bulk micromachined deformable mirrors have been demonstrated, but these mirrors had some challenges that prevented them from being used for laser wavefront control. The mirrors typically have large static aberrations, were susceptible to damage during electrostatic snapdown, and could only be used near room temperature due to the differing materials used in their construction.

During the development of my deformable mirrors we discovered some techniques for achieving good mirror flatness. We developed a technique for bonding the two pieces using an bonding layer that can be annealed so as to only minimally distort the mirror surface. Figure 4 shows the output of a laboratory interferometer before and after the annealing step. After bonding, we consistently measured about a wave of astigmatic aberration over the mirror surface at 633nm, or about 100nm rms distortion. In addition to bonding the two pieces of the deformable mirror together, we developed a technique for attaching standard 2mm ribbon cable connectors to the silicon substrate to allow integration with standard electronics. Several mirrors were measured before bonding to the pad array and they had consistently less than 30nm of rms distortion ($\lambda/50$ at λ=1.55μm).

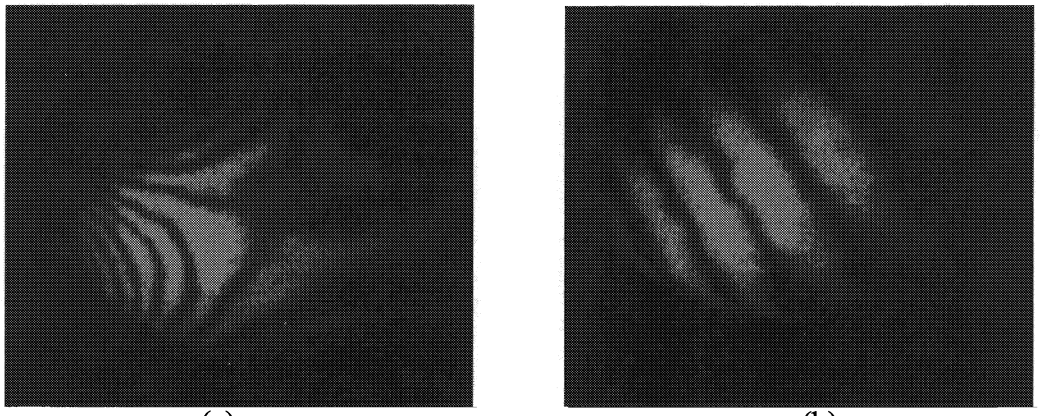

Figure 4 - Inteferogram of the mirror surface (a) before and (b) after annealing the indium bond.

Finally, we developed a technique to eliminate the damaging effects of electrostatic snap-down, which occurs when the electrostatic force exceeds the mechanical force and the two electrostatic pads contact. Most of the damage during electrostatic snap-down occurs when an arc forms between the two pads as the come together. Applying a 1.5-μm coating of a dielectric over the electrostatic pads kept the two pieces from coming close enough to allow for electrostatic breakdown of the dielectric. Roughening the dielectric surface prevented the two pieces from sticking together.

Analytical performance of a membrane deformable mirror were presented by Grosso and Yellin in 1977.[13] They found that the resonance frequencies of a circular membrane in the 0^{th} order angular modes is given by,

$$\nu_{0n} = \left(\frac{\gamma_{0n}}{2a}\right)\sqrt{T/\sigma}$$
$$\gamma_{0n} \cong \beta_{0n} + \left(\frac{2\chi}{\pi^4 \beta_{0n}^3}\right) \qquad (1)$$

where ν_{0n} is the resonance frequency of the n^{th} radial mode, β_{0n} is the root values of the Bessel function of 0^{th} order, T is the tension per length (or stress-thickness product) of the membrane, σ is the mass per area of the membrane, a is the membrane radius, and χ is a measure of the relative importance of the restoring force due to air confined behind the membrane. As an example, a 1-cm diameter 1-μm thick silicon nitride membrane with 50MPa of internal stress and a density of 3100 kg/m^3 has a first resonance at 3.04kHz.

The shape of the deflection of a membrane deformable mirror is given by solving,

$$\nabla^2 Z = -\left(\frac{F(r,t)}{T}\right) \tag{2}$$

where Z is the mirror surface, F(r,t) is the force distribution, and T is the membrane tension. The steady-state deflection of a membrane at a radius r is given by,

$$Z(r) = \frac{F}{2\pi T}\left(\ln\left(\frac{R}{S}\right) + \frac{1}{2S^2}\left(S^2 - r^2\right)\right), 0 < r < S$$
$$Z(r) = \frac{F}{2\pi T}\left(\ln\left(\frac{R}{r}\right)\right), S < r \le R \tag{3}$$

where S is the actuator radius, R is the radius of the membrane, and F is the force. Figure 5 shows the shape of the membrane surface for two different relative actuator sizes.

The analytical theory illustrates two problems with membrane mirrors. First, the resonance frequency of the membrane mirror increases with the membrane size. This means that the membrane mirrors are not scalable to large sizes without sacrificing the temporal performance. Second, the deflection of the mirror is large in extent. Since the influence functions are distributed over the entire mirror surface and electrostatic forces can only attract, the ability to correct for high spatial frequency aberrations is very limited. Despite these limitations, this mirror architecture is sufficient for compensating many types of aberrations. One such application is thermally-induced aberrations in a slab laser amplifier.

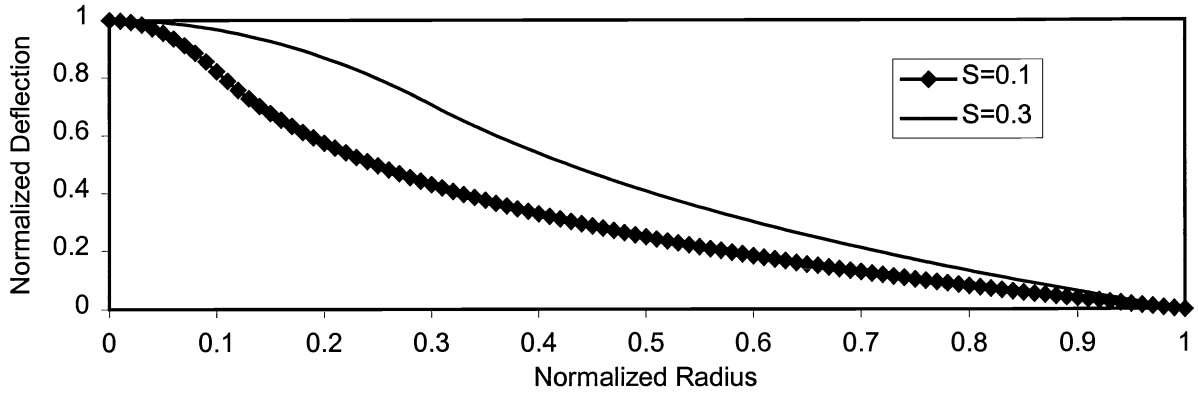

Figure 5 - Shape of the influence function of a membrane deformable mirror for two different relative actuator sizes.

CHARACTERIZATION OF THE SILICON NITRIDE TWO-LAYER DEFORMABLE MIRROR

After characterizing the silicon nitride two-layer deformable mirrors, the mirror driven into Zernike terms using a control computer and a Hartmann sensor for feedback. The Zernike polynomial shapes are used to characterize deformable mirrors because they are commonly used as the basis set for the decomposition of aberrations. The amplitude of the Zernike polynomials is typically compared with the amplitude of the Zernike decomposition of an aberration to determine whether the deformable mirror will be appropriate for wavefront compensation.

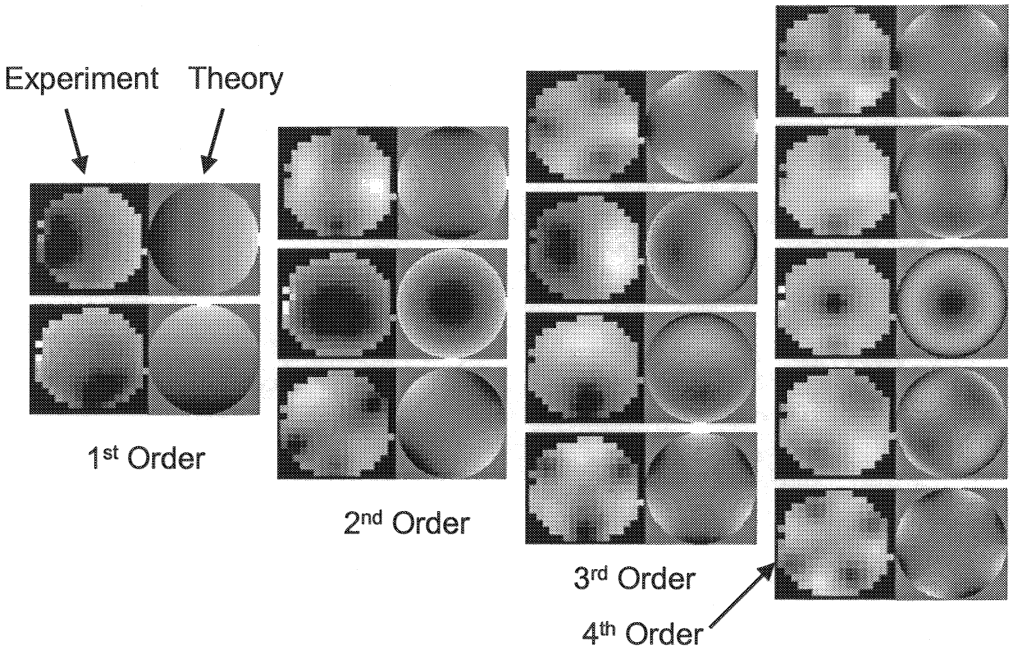

Figure 6 - Measured and theoretical Zernike shapes from the silicon nitride two-layer deformable mirror.

The control computer was programmed to search through error space maximize each Zernike coefficient and minimize the other Zernike coefficients. The error function for this search was the sum of all the Zernike coefficients plus four times the Zernike coefficient being optimized. Figure 6 shows grey-scale plots of the wavefronts measured on a Hartmann sensor and the calculated Zernike shapes adjacent to each other. The tilt term was removed from the wavefronts for the second order and higher terms. The parabolic term was removed from the wavefronts for the third order and higher terms. These terms were removed because the membrane mirrors have a parabolic bias condition, which dominates the mirror shape.

The only major shape difference between the theory and the experiment occurs in the 45 degree astigmatism term, which is the last second-order term. Since the deformable mirror actuators are on a hexagonal grid, the mirror has difficulty getting to a 45-degree astigmatism because the actuators are 30 degrees apart.

We demonstrated the ability of the deformable mirror to be used as a tool for covert optical communications by writing shapes into the spatial phase of a beam of light with the deformable mirror. This demonstration was performed because of the recent interest of the Defense Advanced Research Projects Agency (DARPA) to use deformable mirrors to encode information on beams of light. Figure 7 shows measurements of the aberrations of the spatial phase encoded with letters of the alphabet spelling "STANFOrD" and "INTELLITE". The lower case R was used because the upper case R looked too much like the letter A since I only had 19 actuators on this deformable mirror. The last image in Figure 7 that was written into the spatial phase is a smiley face.

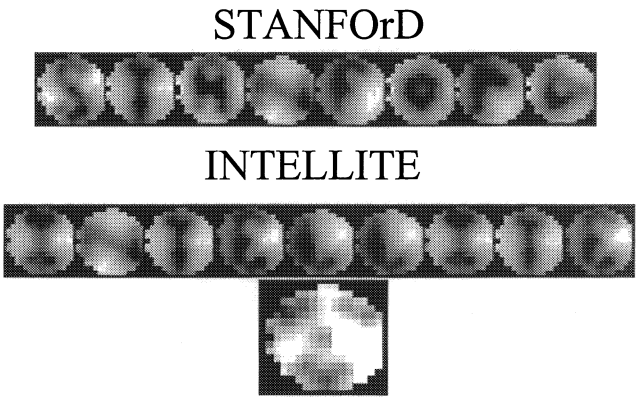

Figure 7 - Measurements on a Hartmann sensor of the spatial phase of a beam of light aberrated with letters of the alphabet and a smiley face.

COMPENSATION OF SLAB LASER AMPLIFIER DISTORTIONS

Figure 8 shows the setup of the MOPA architecture laser with the adaptive optics system. We used an Nd:YAG amplifier slab in the side-pumped geometry in which the pump light enters the slab from the smallest side, the slab is cooled from the largest side, and the laser light bounces between the largest sides.[14] The beam at the deformable mirror was about 5mm in diameter such that the central 7 actuators of the deformable mirror were illuminated and the edge of the mirror was not clipping the beam.

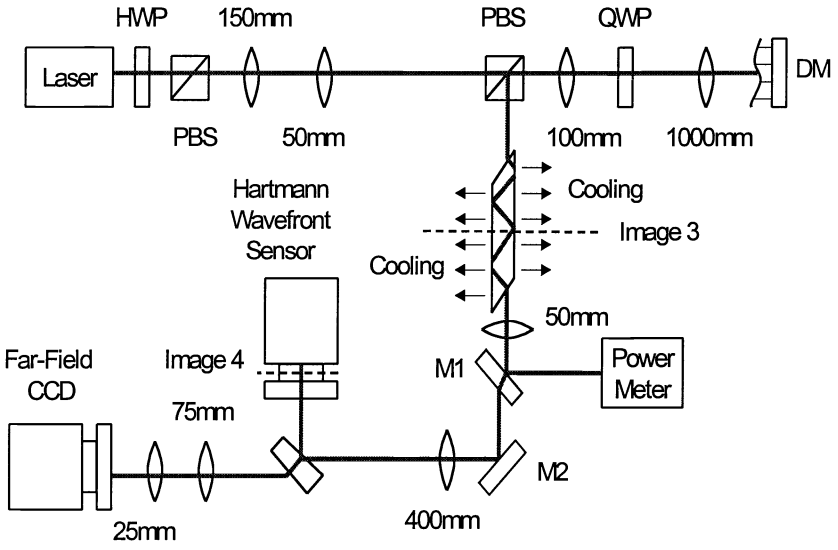

Figure 8 - **Experimental setup of the MOPA architecture laser with active distortion compensation.**

We began by measuring the distortions imposed on the beam due to the thermal load of the pump diodes with a Hartmann wavefront sensor without a deformable mirror in the system. When pumping the amplifier with 175W of 808nm diode light, we found that the amplifier induced 0.81 μm of tilt in one-axis, 0.84 μm of tilt in the other axis, 0.23 μm of focus, 0.35 μm of asigmatism, and 0.075 μm of third-order spherical aberration on a red He-Ne beam illuminating the full 1mm aperture of the slab when performing a 4th order Zernike reconstruction. The other Zernike terms were all less than 60nm in amplitude.

We used a searching algorithm called Genetic Evolution with Simulated Annealing (GESA) to optimize the mirror position and compensate the aberrations because it handled the large inter-actuator crosstalk well. With the GESA algorithm we could vary the optimization parameter.[15] We typically tried to maximize the power in the lowest order Hermite-Gauss (TEM_{00}) mode or minimize the RMS wavefront error, but did some experiments where we simply tried to maximize the power at the far-field CCD as well. The power in the TEM_{00} mode was evaluated by performing the overlap integral on the electric field measured by the Hartmann wavefront sensor.

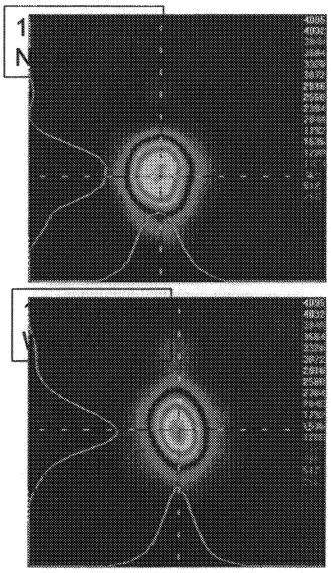

Figure 9 - **Far-field intensity profiles of the laser aberrated by the slab laser amplifier before and after adaptive optics.**

In our first experiment, we optimized the power in the TEM_{00} mode. Before the amplifier was turned on, 92% of the power was in the TEM_{00} mode. By turning on the adaptive optics system and compensating system aberrations, we increased the TEM_{00} power to 95%. By pumping the laser amplifier with 175W of diode light, the power in the TEM_{00} mode decreased to 31%. Engaging the adaptive optic system increased the TEM_{00} mode power to 89%. Figure 9 shows the resulting far-field intensity profiles before and after the adaptive optic loop was closed. The cross-sectional traces shown in white become more gaussian during the loop closure and the center of the beam moves substantially.

In our next experiment, we used the adaptive optics loop to minimize the RMS wavefront error. This experiment yielded similar results with the RMS wavefront error initially at 188nm rising to 377nm after pumping and falling to 195nm after the adaptive optics loop was closed.

THREE-LAYER DEFORMABLE MIRROR ARCHITECTURE

To address the technical challenges of the two-layer mirror architecture, we added a third layer, called the interstitial layer, between the upper mirror membrane and the lower electrodes. **Figure 10** shows the three-layer mirror design. The mirror, the pillars, and the interstitial layer were formed from a single piece of crystalline silicon. The interstitial layer provides a way to generate a local mechanical force upward on each actuator to act against the electrostatic attraction force. The three-layer architecture allows the resonance frequency to be dominated by the stiffness of the interstitial layer and thus allow scaling of the deformable mirror to large apertures. Furthermore, the mechanical force pushing back on the mirror allows for a local deformation to occur, and thus allows the mirror to achieve higher spatial frequency response.

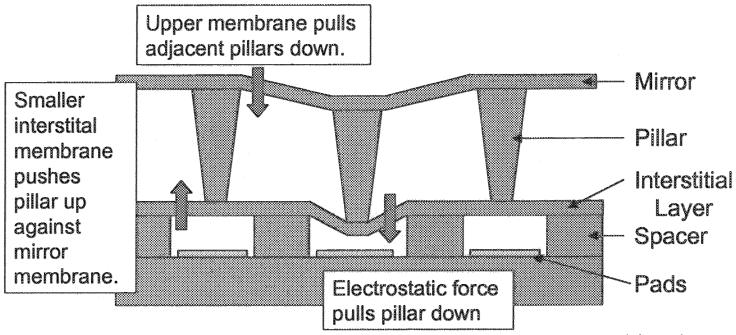

Figure 10 - Diagram of the operation of the three-layer deformable mirror.

We presented this mirror architecture last year[16] after several years of development.[17] The mirror, interstitial layer, and pillars were formed from a single piece of single crystal silicon. The recessed electrodes were fabricated by etching pits in a silicon wafer and depositing gold in these pits. The two pieces were then aligned and bonded together at the edges. Bonding each piece of interstitial layer to each recess is not necessary since any electrostatic force between the pad and the interstitial layer will pull the interstitial layer in contact with the silicon pieces adjacent to the electrodes.

We achieved only about 1 micron of displacement during actuation because the 10 μm-thick pieces of silicon used as the interstitial layer and the mirror surface were excessively stiff. We found the first mechanical resonance frequency at 2 kHz. The measured crosstalk was always less than 30% between actuators.

NEW THREE-LEVEL DEFORMABLE MIRROR ARCHITECTURE

The problem we discovered with the first implementation of this architecture was that the mirror surface was distorted. We solved this problem by slightly modifying the mirror architecture. Figure 11 shows a new three-layer deformable mirror architecture that offers the best potential for achieving all of the desired specifications and an interferogram and wavefront sensor measurement of a mirror built from silicon nitride and silicon in this architecture. The 16 mm diameter mirror surface flatness had only 133nm of wavefront distortion peak-to-valley, mostly in an astigmatic aberration term. We disconnected the interstitial layer from the frame of the mirror and kept the upper surface in tension. Although we are still working on testing this architecture, our initial results show that the mirror flatness is greatly improved.

Either the two-layer or three-layer architecture can be tuned to address many applications by changing the dimensions or materials of the layers, but the three-layer architecture offers more tunability.

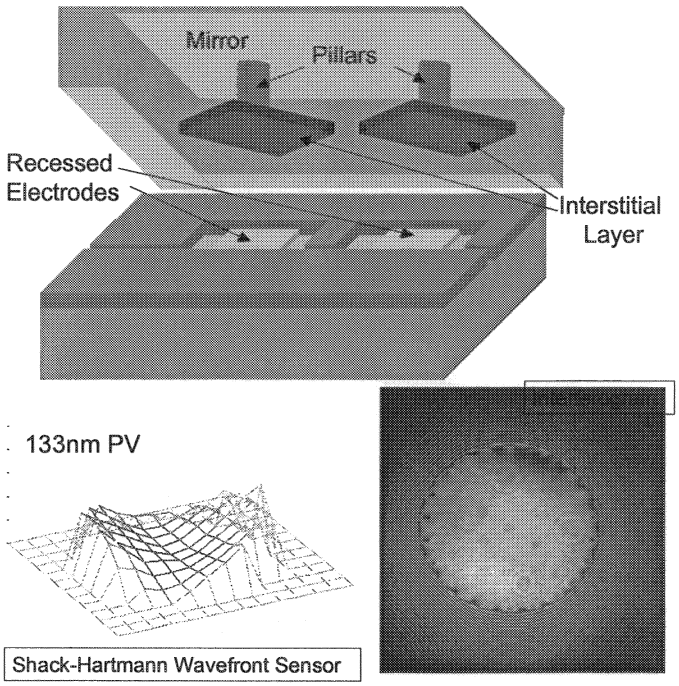

Figure 11 - **New three-layer architecture.**

Generally, any adjustments affect the mechanical stiffness of the interstital layer and the deformable mirror layer. By increasing the stiffness of either layer, its mechanical resonance frequency will increase and its response to applied force decreases. For the three-layer architecture, the ratio of the stiffness of the interstitial layer to the mirror layer allows for tuning the crosstalk.

PISTON-ONLY SCANNING MIRROR

During the research at Stanford, we developed other deformable mirror architectures optimized for other applications. One such mirror was the long-throw piston mirror developed for a standing wave Fourier-transform spectrometer.[18] Figure 12 shows a three-dimensional rendering of the mirror architecture. The open aperture of the frame was 10 mm and the mirror itself was 2mm on a side. The silicon flexures were 22 microns thick. This mirror demonstrated 65 μm of throw when driven on its 700 Hz resonance, which corresponds to about a 2 nm spectral resolution. Due to the slow response of the initial photoconductive detectors, we were only able to achieve about 100nm of spectral resolution. Development of the standing-wave spectrometer is continuing to improve the spectral resolution and the decrease the footprint to the size of a United States Quarter.

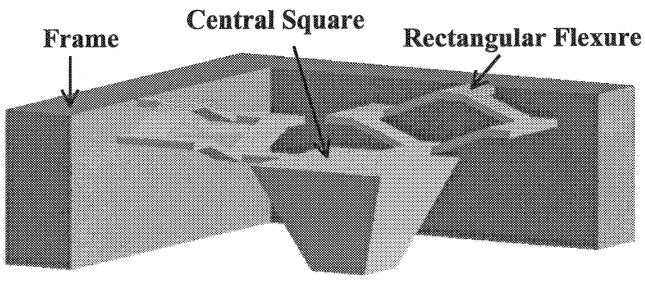

Figure 12 – Three-dimensional rendering of the operation of the piston-only scanning mirror developed for a standing-wave spectrometer. The base of the region labeled "Central Square" is electrostatically attracted to a pad lying underneath.

CONCLUSIONS & FUTURE WORK

Every application of adaptive optics puts different requirements on the deformable mirror, but the two deformable mirror architectures described above have enough flexibility to adapt to almost any application. These mirrors offer a continuous front surface capable of handling reasonable amounts of laser power. The architecture offers enough freedom to enable tuning of all the characteristics over wide ranges.

In the future we imagine the full system integration of adaptive optics onto a single substrate, using silicon photodiodes as detectors, silicon circuitry for the processing of the signals, and a micromachined deformable mirror bonded to the surface for phase correction. To reduce the development cost associated with customizing the mirror architecture to other applications, we are currently developing modeling software to allow us to experiment with different designs before expensive fabrication. We are also making small design changes to the architecture to address new applications.

ACKNOWLEDGEMENTS

We would like to acknowledge the National Science Foundation for their continued support of this research activity. I would like to also acknowledge help on this project from Martin Fejer, Helen Kung, and Sameer Bhaloyta.

REFERENCES

[1] A. Abramovici, W. E. Althouse, R. W. P. Drever, Y. Gursel, S. Kawamura, F. J. Raab, D. Shoemaker, L. Sievers, R. E. Spero, K. S. Thorne, R. E. Vogt, R. Weiss, S. E. Whitcomb, and M. E. Zucker. "LIGO: The Laser Interferometer Gravitational-Wave Observatory", *Science* **256**, pp. 325-33, 1992.

[2] T. J. Kane and R. L. Byer. "Monolithic, unidirectional single-mode Nd:YAG ring laser", *Opt. Letters* **10**, pp. 65-7 1985.

[3] J.D. Mansell, R. L. Byer, and D.R. Neal. "Apodized Micro-lenses for Hartmann Wavefront Sensing" Presented at the Second International Workshop on Adaptive Optics for Industry and Medicine, Durham, England, July 12th-17th, 1999.

[4] R. K. Tyson. *Principles of Adaptive Optics, Second Edition* (Academic, 1998).

[5] A. Kolmogorov. *Turbulence, Classic Papers on Statistical Theory* (Wiley, 1961).

[6] D. L. Fried. "Statistics of a geometric representation of wavefront distortion." *J. Opt. Soc. Am.* **55**, p. 1427, 1965.

[7] D. P. Greenwood. "Bandwidth specification for adaptive optics systems", *J. Opt. Soc. Am.* **67**, p. 390, 1977.
[8] R. H. Hudgin. "Wave-front compensation error due to finite corrector-element size", *J. Opt. Soc. Am.* **67**, p. 393, 1977.
[9] R. K. Tyson. "Theoretical studies of system performance and adaptive optics design parameters", SPIE Vol. 1271, p. 51, 1990.
[10] T. G. Bifano, J. Perreault, R. Krishnamoorthy Mali, and M. N. Horenstein. "Microelectromechanical Deformable Mirrors", *IEEE J. of Sel. Top. In Quan. Elec.* **5**, pp. 83-9, 1999.
[11] M. A. Michalicek, N. Clark, J. H. Comtois, and H. K. Schriner. "Design and simulation of advanced surface micromachined micromirror devices for telescope adaptive optics applications", SPIE Vol. 3353, pp. 805-815, 1998.
[12] J.D. Mansell and R. L. Byer. "Silicon Micromachined Deformable Mirror", SPIE Vol. 3353, pp. 896-901, 1998.
[13] R. P. Grosso and M. Yellin. "The membrane mirror as an adaptive optical element", *J. Opt. Soc. Am.*, **67**, pp. 399-406, 1977.
[14] T. S. Rutherford et al. "Edge-pumped quasi-three-level slab lasers: design and power scaling" *IEEE J. of Quant. Elec.*, **36**, pp. 205-19, 2000.
[15] P. P. C. Yip and Y. Pao. "Growing neural networks using guided evolutionary simulated annealing.", *3rd Annual Conference on Evolutionary Programming* (World Scientific, 1994) , A.V. Sebald and L.J. Fogel, eds., pp. 17-25.
[16] J. D. Mansell, P. B. Catrysse, E. K. Gustafson, and R. L. Byer. "Silicon Deformable Mirrors and CMOS-based Wavefront Sensors", SPIE Vol. 4124, pp. 15-25, 2000.
[17] J. D. Mansell and R. L. Byer. "Silicon Micromachined Deformable Mirror", US Patent 6,108,121.
[18] H. L. Kung, S.R. Bhaloyta, J.D. Mansell, and D. A. B Miller. "Compact Fourier transform spectrometer based on sampling a standing wave", 2000 IEEE/LEOS International Conference on Optical MEMS, pp. 19-20, 2000.